Systematic study of the nuclear capture process using a four-dimensional Langevin dynamical model

Shabnam Mohsina and Jhilam Sadhukhan

Phys. Rev. C **101**, 044607 — Published 16 April 2020

DOI: 10.1103/PhysRevC.101.044607

Systematic study of nuclear capture process using four dimensional Langevin dynamical model

Shabnam Mohsina[1, 2, *] and Jhilam Sadhukhan[1, 2, †]

[1] *Physics Group, Variable Energy Cyclotron Centre, 1/AF Bidhannagar, Kolkata-700064, India*
[2] *Homi Bhabha National Institute, Anushakti Nagar, Mumbai-400094, India*

(Dated: March 23, 2020)

Background: Heavy-ion induced fusion reaction provides the opportunity for synthesizing heavy and superheavy elements in laboratories. In general, the process can be divided in two successive dynamical evolutions. First, a compact dinuclear configuration is formed through capture and then either it decays via quasifission or it equilibrates to a compound nucleus.

Purpose: In this paper, we present a systematic study of nuclear capture process to disentangle the significances of collective angular momentum, target-projectile mass asymmetry, and dissipative forces. Partial contributions from different angular momentum are analyzed for three different reaction channels with ^{16}O, ^{48}Ca, and ^{50}Ti projectiles on the ^{208}Pb target.

Method: A four dimensional Langevin dynamical framework is developed to simulate the time evolution of two colliding nuclei starting from a well separated configuration until a captured composite is formed. The driving potential and the dissipative forces are estimated using the double-folding procedure and the surface friction model, respectively.

Results: Irrespective of target-projectile mass-asymmetry, the dynamics is found to be strongly influenced by the collective angular momentum when it reaches beyond a critical value depending on the beam energy. Effects are more prominent for ^{48}Ca and ^{50}Ti as these systems populate higher angular momenta. Nuclear dissipation is shown to be strongly correlated with the angular momentum.

Conclusions: A deeper understanding of the nuclear dynamics in heavy-ion induced capture process is presented. The importances of target-projectile mass asymmetry, collective angular momentum, and nuclear dissipation are decoupled. This study may provide a better guidance in designing fusion experiments.

I. INTRODUCTION

Heavy-ion induced fusion reaction holds the key to the production of superheavy elements [1, 2]. Substantial experimental and theoretical progresses [1–7] are performed to resolve the intricacies associated with this process. The fusion mechanism can be divided in two categories depending on the incident beam energy. At below-barrier energies, it strongly depends on the channel coupling between the relative motion of the target-projectile composite and intrinsic degrees of freedom. Therefore, the pertinent theoretical model requires a quantum mechanical treatment of the whole process [8–13]. At energies above the fusion barrier, several classical and semiclassical approaches are unveiled. In general, the time evolution can be conceptualized as a two-step process that begins with the formation of a dinuclear system (DNS) through capture or sticking of the target and projectile [14–16]. Subsequently, the DNS either propagates along mass-asymmetry coordinate to form an equilibrated compound nucleus or it decays via quasifission. Therefore, the fusion cross section can be evaluated as a product of capture cross section σ_c and $P_{\rm CN}$, the compound nucleus formation probability which is also known as survival probability.

At present, quantum many-body dynamics based on the time-dependent density functional theory (TDDFT) provides an ideal platform to study above-barrier fusion [17–19]. Albeit very promising, the current implementations of TDDFT can only simulate single fusion/quasifission event: calculation of σ_c and $P_{\rm CN}$ in TDDFT is beyond current computational capabilities, since it would involve large-scale Monte Carlo sampling of all possible entrance channel paths. Fortunately, such a sampling is easily doable within different classical approaches that rely on nuclear dissipation or diffusion. In this case, the time propagation of each event is generated explicitly by solving appropriate equations of motion [15, 20, 21]. Nuclear dissipation strongly influences the dynamics by converting the collective kinetic energy of the composite to its internal excitation energy. For example, in the surface friction model (SFM) [15, 22, 23], σ_c is obtained by employing Langevin dynamical formalism that includes fluctuating and dissipative forces as prescribed by the Einstein's fluctuation-dissipation theorem. In this context, we should mention that σ_c is often calculated using simplistic analytical formulas [24, 25] by approximating the underlying detailed dynamics. The $P_{\rm CN}$ is usually estimated from a statistical model prescription for diffusion over the inner fusion barrier [16, 21, 25].

Numerous theoretical studies are performed to explore different aspects of above-barrier fusion dynamics. A majority of these explains the experimental fusion and quasifission cross sections [15, 16, 25], effect of relative orientation of the deformed target and projectile [21], and

* shabnammohsina652@gmail.com
† jhilam@vecc.gov.in

hindrance due to dissipation [26]. In the present work, we implemented a 4-dimensional (4D) Langevin dynamical model to perform a systematic study of capture process. We closely follow the SFM for this purpose. Specifically, the distributions of collective coordinates are analyzed for different combinations of target-projectile mass asymmetry and collective angular momentum. This study reveals the relative importance of the input parameters and facilitates the choice of entrance channel in producing a particular compound system. We elaborate on the distinct role of nuclear dissipation in different energy and angular momentum regions. Further, the development of a coherent dynamical model description to calculate $P_{\rm CN}$ is under progress.

The present paper is organized as follows. Section II illustrates the 4D Langevin model. The calculated results are analyzed in Sec. III. Possibility of evaporation of light particles and mass transfer during the capture process are described in Sec. IV and Sec. V, respectively. Finally, we conclude in Sec. VI.

II. THEORETICAL MODEL

The expression for the nuclear capture cross section can be written as [26],

$$\sigma_c = \frac{\pi\hbar^2}{2\mu E_{\rm c.m.}}\sum_{\ell=0}^{\infty}(2\ell+1)T_\ell \simeq \frac{\pi\hbar^2}{2\mu E_{\rm c.m.}}\int_0^{\infty}(2\ell+1)T_\ell d\ell \tag{1}$$

where μ and $E_{\rm c.m.}$ are the reduced mass and initial center of mass energy of the composite, respectively. The initial angular momentum is represented with ℓ. The partial capture cross section can be expressed in terms of the transmission coefficient T_ℓ as,

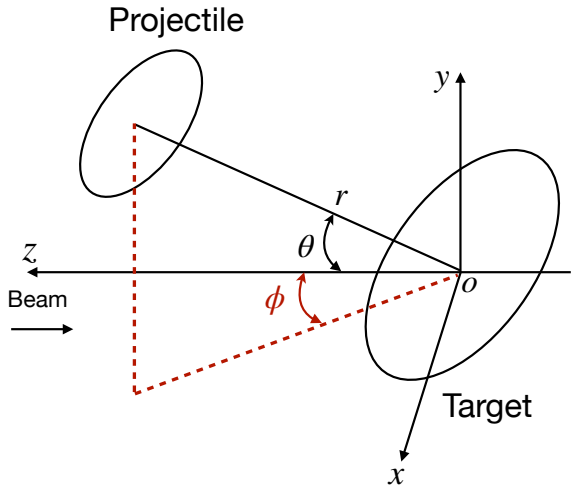

FIG. 1. (Color online) Schematic of relative coordinates of target and projectile.

$$\frac{d\sigma_c(\ell)}{d\ell} = \frac{\pi\hbar^2}{2\mu E_{\rm c.m.}}(2\ell+1)T_\ell. \tag{2}$$

We calculate T_ℓ by solving a stochastic Langevin dynamical model. In general, multidimensional Langevin equations are written as [26],

$$\begin{aligned}\frac{dp_i}{dt} =& -\sum_{jk}\frac{p_jp_k}{2}\frac{h_jh_k}{h_i}\frac{\partial}{\partial q_i}(\mathcal{M}^{-1})_{jk} - \frac{1}{h_i}\frac{\partial V}{\partial q_i}\\ &-\sum_{jk}K_{ij}\left(\mathcal{M}^{-1}\right)_{jk}p_kh_k + \sum_j g_{ij}\Gamma_j(t),\\ \frac{dq_i}{dt} =& \sum_j\left(\mathcal{M}^{-1}\right)_{ij}p_jh_j,\end{aligned} \tag{3}$$

where q_i represents a generalized coordinate and p_i is the conjugate momentum. Here, h_is are the Lamé coefficients associated to generalized coordinates. $\mathcal{M}$ and K are the collective inertia tensor and the dissipation tensor, respectively. Time-correlation property of the random force is assumed to follow the relation: $\langle\Gamma_i(t)\Gamma_j(t')\rangle = 2\delta_{ij}\delta(t-t')$, and the strength g_{ij} is related to the dissipation coefficient K_{ij} through the fluctuation-dissipation theorem: $g_{ik}g_{kj} = K_{ij}T$; T being the temperature of the composite.

In the present work, the collective coordinates are chosen to be $(q_1,q_2,q_3,q_4) \equiv (r,\theta,\beta_1,\beta_2)$, where r is the distance between the centre of masses of the target and projectile, θ is the angle made by r with the axis parallel to the incoming beam, and β_1 and β_2 define the axial quadruploe deformations of target and projectile, respectively. As shown in Fig. 1, (r,θ,ϕ) forms a spherical polar coordinate system with the origin at the center of mass of the target. The dynamics along ϕ is trivial since the initial deformations are assumed to be negligible. Also, the initial collective energy is fully coupled to the r and θ motions. Hence, the mass asymmetry of the composite is believed to be preserved during the course of capture. This assumption is validated in Sec. V. In the 4D hyperspace, $(h_1,h_2,h_3,h_4) = (1,r,1,1)$. The inertia tensor has the following diagonal form,

$$\mathcal{M} = \begin{pmatrix}\mu & 0 & 0 & 0\\ 0 & \mu r^2 & 0 & 0\\ 0 & 0 & B_1 & 0\\ 0 & 0 & 0 & B_2\end{pmatrix}, \tag{4}$$

where B_1 (B_2) is the liquid drop mass parameter corresponding to the quadrupole deformation β_1 (β_2). The dissipation tensor, K is calculated using the surface friction model as described in [26]. It is symmetric having the components:

$$\begin{aligned}K_{rr} =& K_r^0\left(\frac{\partial V_N}{\partial r}\right)^2,\\ K_{\theta\theta} =& K_\theta^0\left(\frac{\partial V_N}{\partial r}\right)^2,\\ K_{\beta_i\beta_j} =& R_iR_jY_{20}^2(0)K_{rr} + \delta_{ij}K_\beta^0\sqrt{C_jB_j},\\ K_{r\beta_i} =& -2R_iY_{20}(0)K_{rr},\end{aligned} \tag{5}$$

and all the other components are zero. Here, V_N is the potential energy derived from the isospin independent part of the target-projectile interaction, R_1 (R_2) is the equivalent spherical radius of the target (projectile) nucleus, and C_i is the liquid drop stiffness parameter corresponding to the deformation β_i. The $Y_{20}(0)$ is the normalized spherical harmonic calculated on the symmetry axis of a nucleus. The values of the constant friction parameters are $K_r^0 = 3.5\times10^{-23}$ s/MeV, $K_\theta^0 = 0.01\times10^{-23}$ s/MeV, and $K_\beta^0 = 20$. Incorporating the $\mathcal{M}$ and K tensors in Eq. 3 we get,

$$\begin{aligned}
\frac{dp_r}{dt} =& \frac{\ell^2}{\mu r^3} - \frac{\partial V_{12}}{\partial r} - K_{rr}\frac{p_r}{\mu} - \sum_i K_{r\beta_i}\frac{\pi_i}{B_i} + g_{rr}\Gamma_r(t),\\
\frac{dr}{dt} =& \frac{p_r}{\mu},\\
\frac{1}{r}\frac{d\ell}{dt} =& -K_{\theta\theta}\frac{\ell}{\mu r} + g_{\theta\theta}\Gamma_\theta(t),\\
\frac{d\theta}{dt} =& \frac{\ell}{\mu r^2},\\
\frac{d\pi_i}{dt} =& -\frac{\partial}{\partial\beta_i}\left(V_{12} + \frac{1}{2}C_i\beta_i^2\right) - K_{r\beta_i}\frac{p_r}{\mu} - \sum_j K_{\beta_i\beta_j}\frac{\pi_j}{B_j}\\
&+ g_{\beta_i\beta_i}\Gamma_{\beta_i}(t),\\
\frac{d\beta_i}{dt} =& \frac{\pi_i}{B_i},
\end{aligned} \tag{6}$$

where p_r and $\pi_i (i = 1, 2)$ are the momentum conjugate to r and β_i, respectively. The equation for π_i additionally contains the restoring force associated to the surface vibration along β_i. We have neglected fluctuations coupled to the off-diagonal terms of the dissipation tensor as their effects are small [27].

The driving potential V_{12} is calculated by adding the contributions from nuclear (V_N), Coulomb (V_C) and rotational (V_R) energies of the composite. The V_N is obtained by double folding the effective Migdal interaction with nuclear densities. The resulting expression is [21],

$$V_N(r,\beta_1,\beta_2) = \int \rho_1(\vec{r}';\beta_1) f_{eff}(\vec{r}')\rho_2(\vec{r}'-\vec{r};\beta_2)d^3r' \tag{7}$$

where ρ_1 and ρ_2 are the mass densities of the target and projectile, respectively, as given by the Wood-Saxon distribution [21]. The effective nucleon-nucleon force is given by

$$f_{eff}(\vec{r}') = 300\left(f_{in} + (f_{ex} - f_{in})\frac{\rho(0)-\rho(\vec{r}')}{\rho(0)}\right) \tag{8}$$

where $\rho = \rho_1 + \rho_2$, $f_{in} = 0.09$, and $f_{ex} = -2.59$ [21]. The Coulomb potential between two uniformly charged deformed nuclei is given by [28],

$$V_C(r,\beta_1,\beta_2) = \frac{Z_1Z_2e^2}{r} + \frac{Z_1Z_2e^2}{r^3}V_C' \tag{9}$$

with

$$V_C' = \sum_{i=1}^{2}\left\{\sqrt{\frac{9}{20\pi}}R_i^2\beta_i + \frac{3}{7\pi}(R_i\beta_i)^2\right\}.$$

The rotational energy is calculated from the quantum mechanical expression,

$$V_R = \frac{\hbar^2\ell(\ell+1)}{2\mu r^2}. \tag{10}$$

In the present work, we consider spherical target and projectiles and hence V_{12} is independent of initial orientations. Both the nuclei can acquire deformation in the course of dynamics and the corresponding symmetry axes are always considered to be along r.

We solve Langevin equations (Eq. 6) using finite difference method with a time step of $\delta t = 0.0005\hbar$/MeV. The temperature T (in MeV) of the composite is calculated using the Fermi gas model: $T = \sqrt{E^*/a}$; a being the level density parameter which is assumed to be $A/10$ for the present purpose. The excitation energy, E^* is produced through dissipation of the collective kinetic energy. At each time-step, we calculate E^* from the conservation of total energy as,

$$E^* = E_{\rm c.m.} - \left(\frac{p_r^2}{2\mu} + \sum_i \frac{\pi_i^2}{2B_i} + V_{12}(r,\beta_1,\beta_2)\right). \tag{11}$$

An ensemble of Langevin trajectories is calculated for each macrostate specified by $(E_{\rm c.m.}, \ell, r(t=0))$. The initial r is chosen sufficiently large such that there is no overlap of nuclear densities and the fluctuation-dissipation component is absent ($E^* = 0$). In addition, π_is are assumed to be zero at the beginning ($t = 0$) and $E_{\rm c.m.}$ is fully shared between p_r and V. Therefore, both the initial p_r and ℓ can be determined uniquely form the initial r and θ. The fate of a Langevin trajectory is decided from the magnitude and direction of p_r. We judge a trajectory as capture-event by satisfying the boundary condition: $p_r\,|_{r<r_b} \simeq 0$, where r_b is the value of r at the peak of the potential barrier. For an unsuccessful capture, p_r increases with r ($> r_b$) due to Coulomb repulsion. In an ensemble of N^t Langevin trajectories, if N^c represents the number of DNS formed then,

$$T_\ell = \frac{N^c}{N^t}. \tag{12}$$

In addition to the capture cross section, we calculate ensemble averages of the dynamical coordinates at the time of capture ($t = t^c$),

$$\langle q_i^c\rangle = \frac{\sum_k (q_i^c)_k N_k^c}{\sum_k N_k^c} = \frac{\sum_k (q_i^c)_k N_k^c}{N^c}, \tag{13}$$

where N_k^c is the number of DNS with the outcome $(q_i^c)_k$ for the observable q_i. The superscript c indicates the final value of q_i at $t = t^c$.

For a simplified calculation, T_ℓ is often parametrized as,

$$T_\ell^p = \frac{1}{1+\exp\left(\frac{\ell-\ell_{cr}}{\delta\ell}\right)}. \tag{14}$$

The parameters ℓ_{cr} and $\delta\ell$ are derived in [29] by fitting the capture cross-section of the ^{19}F+^{181}Ta reaction. The corresponding expression for ℓ_{cr} is [26],

$$\ell_{cr} = \sqrt{\frac{A_1 A_2}{A_1 + A_2}}(A_1^{1/3} + A_2^{1/3})F(x) \qquad (15)$$

with

$$F(x) = \begin{cases} (0.33 + 0.205\sqrt{x}) & \text{if } 0 < x < 120 \\ 2.5 & \text{if } x > 120, \end{cases} \qquad (16)$$

$x = E_{\rm c.m.} - V_c$ in MeV; V_c being the Coulomb barrier

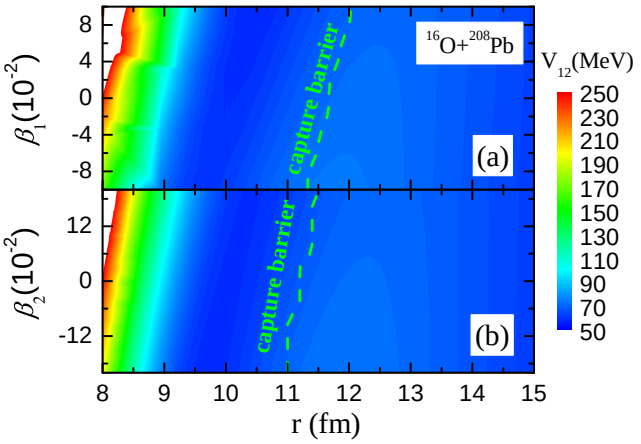

FIG. 2. (Color online) Projection of potential energy, on the (a) $\beta_1 = 0$ and (b) $\beta_2 = 0$ surfaces, calculated for the ^{16}O + ^{208}Pb reaction. Capture barrier contours are indicated by dashed lines

given by: $V_c = 1.1755 Z_1 Z_2/(R_1 + R_2 + 1.6)$ in MeV. The diffuseness $\delta\ell$ is formulated as,

$$\delta\ell = \begin{cases} 10^{-5}(A_1A_2)^{3/2}\,[1.5 + 0.02(x-10)] & \text{if } x > 10 \\ 10^{-5}(A_1A_2)^{3/2}\,[1.5 - 0.04(x-10)] & \text{if } x < 10. \end{cases} \qquad (17)$$

Here, A_1 (Z_1) and A_2 (Z_2) are mass numbers (atomic numbers) of the target and projectile, respectively.

III. RESULTS

We have studied three reaction channels: (i) ^{16}O+^{208}Pb, (ii) ^{48}Ca+^{208}Pb, and (iii) ^{50}Ti+^{208}Pb, where the target and projectiles are assumed to be spherical at their ground state. The channel (i) is reasonably asymmetric with a comparatively light projectile that minimizes the chances of quasifission and, therefore, most of the captured events emerge to complete fusion. The other two channels are known to contribute in the quasifission process [30]. First, we study the deformation dependence of the potential energy V_{12}. Two-dimensional projections of V_{12} are plotted in Fig. 2 alternately for

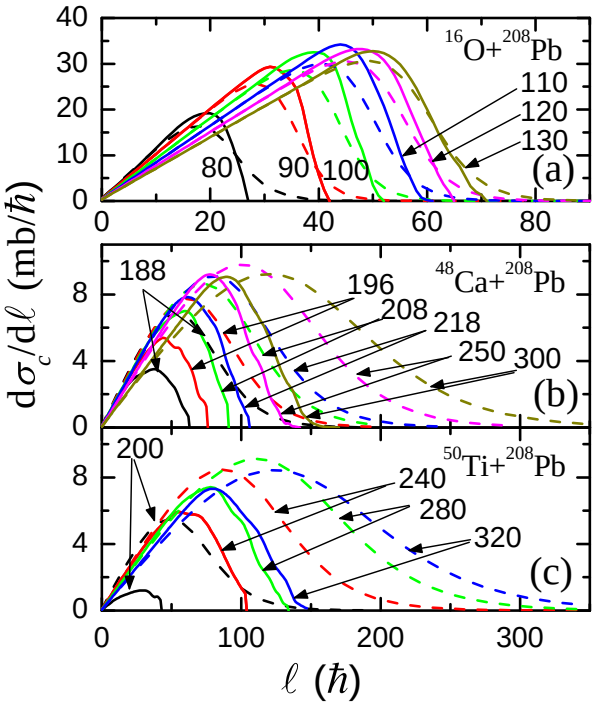

FIG. 3. (Color online) Variation of $\frac{d\sigma_c}{d\ell}$ with ℓ calculated for (a) ^{16}O+^{208}Pb, (b) ^{48}Ca+^{208}Pb, and (c) ^{50}Ti+^{208}Pb reactions. Solid and dashed lines represent Langevin dynamical calculations and systematics (see text), respectively, for different $E_{\rm c.m.}$ (in MeV) as indicated.

fixed β_1 and β_2. Compared to the strong r dependence, V_{12} remains very flat along β_1 and β_2. Therefore, β_1 and β_2 are expected to play a minor role in capture dynamics.

Figure 3 shows the partial capture cross section (Eq. 2) calculated for different $E_{\rm c.m.}$. The dynamical results are compared with the approximate formula where T_ℓ is replaced with T_ℓ^p. Although there is a reasonable agreement for the channel (i), T_ℓ^p drastically overestimates the dynamical results in case of the heavy projectiles (channel (ii) and (iii)). The parameters ℓ_{cr} and $\delta\ell$ can be adjusted to mimic the dynamical capture cross section σ_c (Eq. (1)). However, a major disadvantage of Eq. (14) is that the shape of dynamical $d\sigma_c/d\ell$ can not be reproduced near the high ℓ tail region where $T_\ell < 1$. Specifically, in comparison to $d\sigma_c/d\ell$ obtained from T_ℓ^p, the dynamical $d\sigma_c/d\ell$ shows a steeper descent along the ℓ-axis predicting the absence of very large ℓ values in captured events. Hence, the simplified prescription of Eq. (14) should not be used, especially for heavy projectiles with mass ≈40 or more, to estimate ℓ distribution of captured events. This is an important outcome of our calculation as the formation of a fully equilibrated compound system strongly depends on the ℓ-population. The deviation of dynamical results from the systematics is a manifestation of dissipative effect that prevents Langevin trajectories from overcoming the capture barrier at a high value of ℓ.

The dynamical $d\sigma_c/d\ell$ contains small fluctuations in

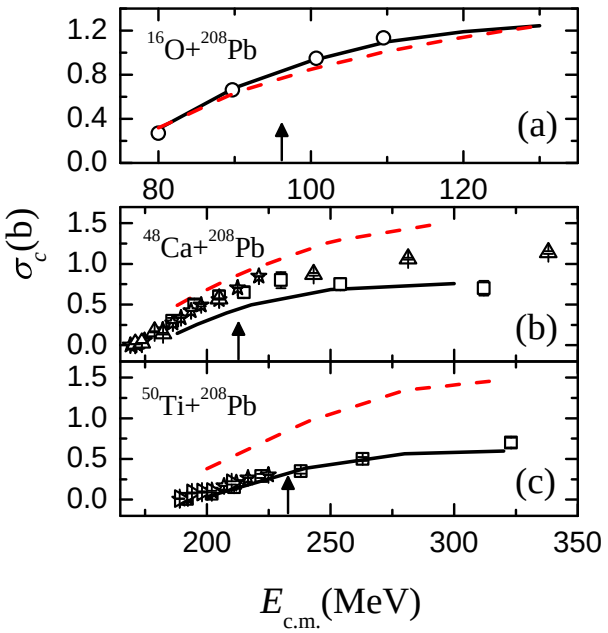

FIG. 4. Capture cross sections calculated from Langevin dynamics (solid lines) and systematics (dashed lines) are compared with experimental data (circle [31], triangle [32], square[33], star [7], and right triangle [34]). Coulomb barrier energies are indicated on x-axes with arrows. Reaction channels are mentioned in each panel.

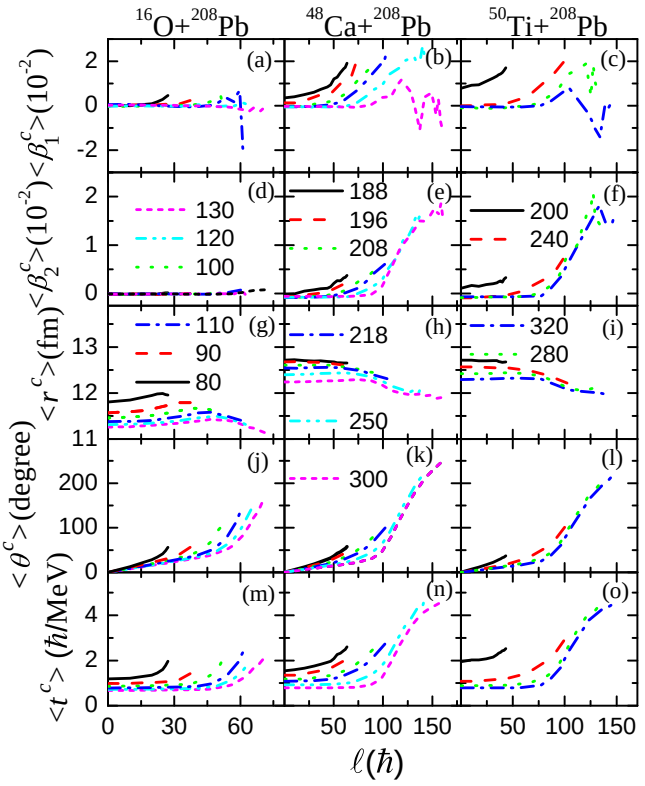

FIG. 5. (Color online) Variations of ensemble averages of collective coordinates ($\langle\beta_1^c\rangle$ in (a)-(c), $\langle\beta_2^c\rangle$ in (d)-(f), $\langle r^c\rangle$ in (g)-(i), and $\langle\theta^c\rangle$ in (j)-(l)) and capture time $\langle t^c\rangle$ ((m)-(o)) with angular momentum ℓ. Different lines correspond to different $E_{\rm c.m.}$ (in MeV) as mentioned. Reaction channels are given on top of each column.

the $T_\ell < 1$ region. These statistical fluctuations appear due to low N^c counts. We considered $N^t = 25,000$ for each ensemble $(A_{\rm DNS}, Z_{\rm DNS}, E_{\rm c.m.}, \ell)$ and the corresponding statistical error is marginal when $N^c \approx N^t$. However, N^c decreases sharply near the tail of $d\sigma_c/d\ell$ and in most cases, $N^c < 100$ for $T_\ell < 0.5$. The present limitation of N^t is imposed by the availability of computational resources. Typically, calculation of a single $d\sigma_c/d\ell$ curve requires $\approx 1,50,000$ cpu hours of computational time with a simultaneous use of 1000 processors in a high-performance computer.

We calculated σ_cs from $d\sigma_c/d\ell$ and compared it with the experimental data in Figure 4. Evidently, the Langevin results closely follow the experimental values for (i) and (iii). In case of (ii), both the target and projectile are doubly magic nuclei. Hence, the observed mismatch, specifically at lower energies, may be attributed to strong shell effects. The shell effects are neglected in the present work as we mainly consider beam energies well above the potential barrier height. The excitation functions of σ_c, obtained from T_ℓ^ps of (i), (ii), and (iii), do not reproduce the experimental values. It validates the importance of dissipative dynamics in predicting the correct nature of $d\sigma_c/d\ell$ vis-á-vis σ_c. Although the discrepancy is small for (i), a precise calculation of the tail part of $d\sigma_c/d\ell$ is required for an accurate estimation of σ_c.

Subsequently, we calculate ensemble averages of the capture time t^c and all the collective coordinates at $t = t^c$. These are demonstrated in Fig. 5 as functions of ℓ. Irrespective of $E_{\rm c.m.}$, ℓ, and mass asymmetry of DNS, $\langle\beta_1^c\rangle$ and $\langle\beta_2^c\rangle$ remain almost constant at their initial value of 0. The restoring force provided by C_i is strong enough to resist any shape change. Although this observation is supposed to break at a high beam energy, the dynamics along deformation coordinates may safely be neglected for cold fusion reactions. In fig. 5, $\langle r^c\rangle$ defines the average r at $t = t^c$ and, as the figure shows, it changes marginally with ℓ. However, $\langle r^c\rangle$ decreases with $E_{\rm c.m.}$ since the collective kinetic energy drives the DNS to a more compact configuration. Next, we describe $\langle\theta^c\rangle$ that measures the amount of orbiting before DNS is formed. θ^c governs the angular distribution of non-compound events which decay within a very short span of time after capture. Precisely, the correlation between angular distribution and angular momentum of these fast-decaying events can be understood from $\langle\theta^c\rangle$. As depicted in Fig. 5, initially $\langle\theta^c\rangle$ increases linearly with ℓ and then it rises sharply as $d\sigma_c/d\ell$ starts reducing to zero. For (ii) and (iii), vary large values of ℓ ($> 100\ \hbar$) are populated that stimulate significant amount of orbiting. This can be explained as follows. For a fixed incident

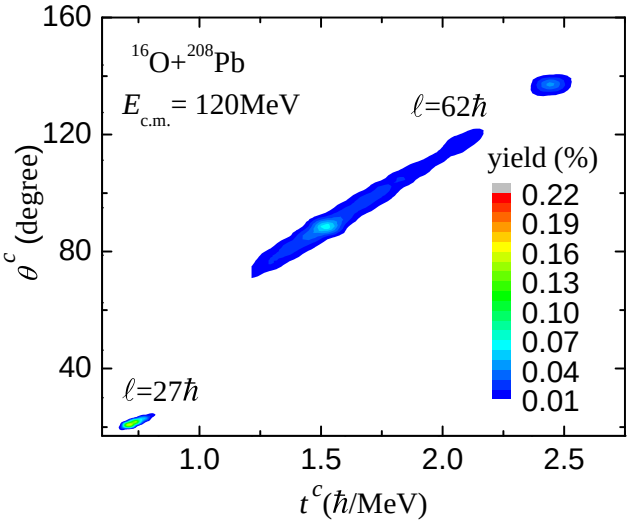

FIG. 6. (Color online) Capture yield distribution of ^{16}O + ^{208}Pb reaction for two different initial angular momentum (ℓ).

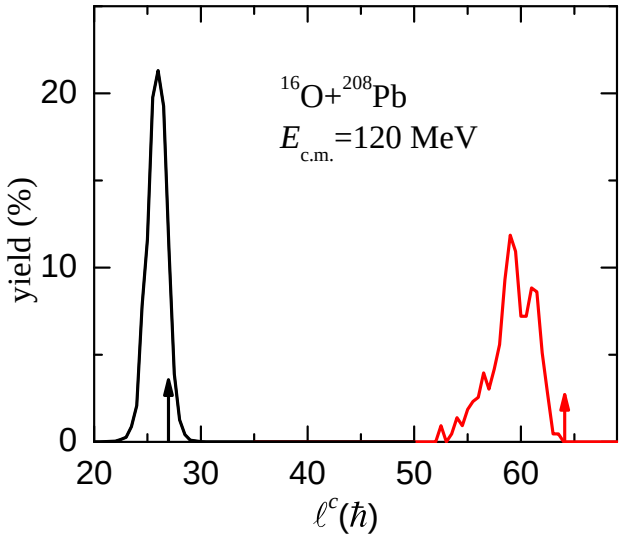

FIG. 7. (Color online) Capture yield distribution as a function of final angular momentum (ℓ^c) plotted for two initial angular momenta (ℓ) indicated by arrows.

energy ($E_{\rm c.m.}$), the radial momentum, which decides the capture time, is comparatively small near the terminal values of ℓ. It helps the composite to rotate more during the slow propagation towards DNS. The corresponding $\langle t^c \rangle$, plotted in Fig. 5, supports this argument. Also, a comparison of $\langle \theta^c \rangle$ for the three reactions concludes that it depends only on the amount of ℓ induced, but there is no intrinsic dependency on the target-projectile mass asymmetry.

For a deeper understanding of the correlation between θ^c and t^c, the DNS yield distributions corresponding to different final states specified with (θ^c, t^c) are elucidated in Fig. 6. For the smaller value of ℓ corresponding to $T_\ell \simeq 1$, the distribution is well localized in both the directions suggesting a marginal role of dispersion. In contrast, at the higher ℓ ($T_\ell \simeq 0$), the ranges of θ^c and t^c are broad. However, the width of the distribution is pretty narrow due to strong correlation between t^c and θ^c. A similar behavior is observed for the other systems. This establishes the critical role of fluctuation-dissipation in determining the high-ℓ part of $d\sigma_c/d\ell$ that tunes the capture cross section.

Finally, we investigate the impact of dissipation along θ. The capture barrier vanishes above a certain ℓ (say ℓ_m) because of the centrifugal force; precisely, ℓ defines the initial angular momentum of the composite. Then, DNS formation is possible if the initial ℓ reduces to a value for which the potential pocket reappears. This reduction is primarily controlled by the fluctuation-dissipation, whereas the conservative force is weak enough to produce such an effect. Figure 7 shows the dispersion in ℓ^c (value of ℓ at $t = t^c$) for two extreme values of ℓ. As evident, the distribution is symmetric and narrower for the lower ℓ. The higher ℓ is chosen to be more than ℓ_m. As a result, the yield distribution is quite asymmetric with no events at and above the ℓ. Also, irrespective of the system we found that the width of the distribution is more for a ℓ close to ℓ_m. It again signifies the importance of dissipative forces for high angular momenta near the edge of $d\sigma_c/d\ell$.

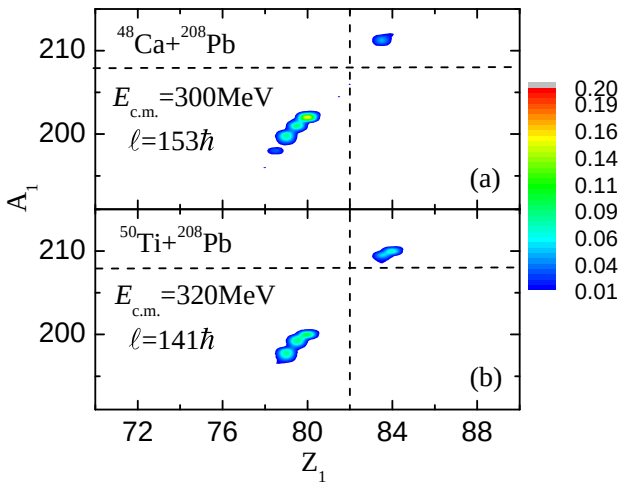

FIG. 8. Fraction of captured events with target mass A_1^c and target charge Z_1^c at t^c. Dotted lines indicate initial A_1 and Z_1. Values of $E_{\rm c.m.}$, initial ℓ and reactions are mentioned in each panel.

IV. PARTICLE EVAPORATION IN CAPTURE

We have investigated the possibility of pre-equilibrium evaporation of light particles during the capture process. Emission of neutron, proton, α, and γ-ray are considered

at each time step. The particle emission widths are calculated using the Weisskopf's statistical model prescription [35]. The excitation energy for the particle evaporation is generated through the dissipation of collective kinetic energy. Particle emissions are found to be highly improbable during the short span of capture dynamics. Moreover, a moderate amount of excitation energy builds up only at the end stage of dynamics. A detail study of pre-equilibrium emission in the post-capture evolution is under progress.

V. POSSIBILITY OF MASS FLOW

We have mentioned earlier that mass flow between the target and projectile can be neglected during the capture process and this mass rearrangement takes place as a subsequent dynamical evolution with a comparatively slower time scale. This assumption is followed in various other theoretical models [14, 16, 21]. However, for a quantitative understanding, we have estimated the amount of mass transfer during the capture process. To this end, we solved overdamped Langevin equation along the mass asymmetry coordinate (α). The associated equation is given by,

$$\frac{d\alpha}{dt} = -\frac{1}{K_{\alpha\alpha}}\frac{\partial V_{12}}{\partial \alpha} + g_{\alpha\alpha}\Gamma_{\alpha}(t), \tag{18}$$

where $\alpha = |Z_1 - Z_2|/(Z_1 + Z_2)$ that measures the target-projectile charge asymmetry (for each combination of (Z_1, Z_2; $Z_1 + Z_2 = Z_{\rm DNS}$), the corresponding masses (A_1, A_2; $A_1 + A_2 = A_{\rm DNS}$) are uniquely determined by maximizing the total binding energy of the DNS) and V_{12} is the multidimensional potential energy [21] extended along α for the present purpose. We incorporated the above equation in the original set of Langevin equations (Eq. 6) and the dynamics along β_1 and β_2 are neglected as these hardly affect during capture. Therefore, the time evolution is simulated with three coordinates - r, θ, and α. The strong friction limit is applicable as the initial collective kinetic energy associated to α is zero and the mass transfer takes place only due to fluctuations in α. As explained in a previous section, we have neglected the off-diagonal terms in Eq. 18. Also, the dissipation strength $K_{\alpha\alpha}$ is assumed to be constant at $50\hbar$ which is obtained in compliance with K_{rr}.

We have performed the calculations for extreme values of ℓ where the chances of mass transfer is higher because of long capture time. The mass number (A_1^c) and the atomic number (Z_1^c) of the target nucleus at the time of capture are shown in Fig. 8 for two sample cases of ^{48}Ca and ^{50}Ti projectiles. As evident, even at these high ℓ, the mass and charge transfer fractions are $< 6\%$ and $< 5\%$, respectively. Moreover, the contribution of these ℓ in the capture cross section is small. Therefore, the capture process is hardly effected due to the internuclear mass transfer. In addition, Fig. 8 indicates that, both for ^{48}Ca and ^{50}Ti, a majority of the events tends to move toward mass-symmetric DNS (i.e. both A_1 and Z_1 decreases from their original values). These events eventually contributes in the quasifission channel.

VI. CONCLUSION

We presented a 4-dimensional Langevin dynamical model to study nuclear capture process. The model is benchmarked with the experimentally known capture cross sections. Independent behavior of all of the four collective coordinates are extracted for various energy, angular momentum, and entrance channel mass asymmetry. Relative importance of these coordinates is discussed and nuclear deformations are found to be insensitive to the capture dynamics. Of course, the cross section depends on the relative orientation of the target and projectile in case of deformed nuclei [21]. We did not notice any direct dependency on mass asymmetry except the fact that heavier projectiles induce large angular momentum to the dinuclear system. Specifically, the dynamical evolutions are described to be almost identical for the three reaction channels at a particular angular momentum and beam energy. Further, strong correlation between the capture time and nuclear orbiting is established. The role of nuclear dissipation in different angular momentum regions is investigated. It is observed that dissipation plays a pivotal role in ascertaining the shape of the partial capture cross section which essentially determines the total capture cross section. The present findings give a guidance in selecting the target and projectile for heavy ion induced fusion reaction.

ACKNOWLEDGMENTS

The authors acknowledge the computation time provided by the Computing Facilities of Variable Energy Cyclotron Centre. Also, a part of the computing support for this work came from the Lawrence Livermore National Laboratory (LLNL) Institutional Computing Grand Challenge program.

[1] S. Hofmann and G. Münzenberg, Rev. Mod. Phys. **72**, 733 (2000).

[2] S. A. Giuliani, Z. Matheson, W. Nazarewicz, E. Olsen, P.-G. Reinhard, J. Sadhukhan, B. Schuetrumpf, N. Schunck, and P. Schwerdtfeger, Rev. Mod. Phys. **91**, 011001

(2019).
[3] C. Golabek and C. Simenel, Phys. Rev. Lett. **103**, 042701 (2009).
[4] Y. T. Oganessian, F. S. Abdullin, P. D. Bailey, D. E. Benker, M. E. Bennett, S. N. Dmitriev, J. G. Ezold, J. H. Hamilton, R. A. Henderson, M. G. Itkis, Y. V. Lobanov, A. N. Mezentsev, K. J. Moody, S. L. Nelson, A. N. Polyakov, C. E. Porter, A. V. Ramayya, F. D. Riley, J. B. Roberto, M. A. Ryabinin, K. P. Rykaczewski, R. N. Sagaidak, D. A. Shaughnessy, I. V. Shirokovsky, M. A. Stoyer, V. G. Subbotin, R. Sudowe, A. M. Sukhov, Y. S. Tsyganov, V. K. Utyonkov, A. A. Voinov, G. K. Vostokin, and P. A. Wilk, Phys. Rev. Lett. **104**, 142502 (2010).
[5] J. Khuyagbaatar, A. Yakushev, C. E. Düllmann, D. Ackermann, L.-L. Andersson, M. Asai, M. Block, R. A. Boll, H. Brand, D. M. Cox, M. Dasgupta, X. Derkx, A. Di Nitto, K. Eberhardt, J. Even, M. Evers, C. Fahlander, U. Forsberg, J. M. Gates, N. Gharibyan, P. Golubev, K. E. Gregorich, J. H. Hamilton, W. Hartmann, R.-D. Herzberg, F. P. Heßberger, D. J. Hinde, J. Hoffmann, R. Hollinger, A. Hübner, E. Jäger, B. Kindler, J. V. Kratz, J. Krier, N. Kurz, M. Laatiaoui, S. Lahiri, R. Lang, B. Lommel, M. Maiti, K. Miernik, S. Minami, A. Mistry, C. Mokry, H. Nitsche, J. P. Omtvedt, G. K. Pang, P. Papadakis, D. Renisch, J. Roberto, D. Rudolph, J. Runke, K. P. Rykaczewski, L. G. Sarmiento, M. Schädel, B. Schausten, A. Semchenkov, D. A. Shaughnessy, P. Steinegger, J. Steiner, E. E. Tereshatov, P. Thörle-Pospiech, K. Tinschert, T. Torres De Heidenreich, N. Trautmann, A. Türler, J. Uusitalo, D. E. Ward, M. Wegrzecki, N. Wiehl, S. M. Van Cleve, and V. Yakusheva, Phys. Rev. Lett. **112**, 172501 (2014).
[6] B. B. Back, H. Esbensen, C. L. Jiang, and K. E. Rehm, Rev. Mod. Phys. **86**, 317 (2014).
[7] K. Banerjee, D. J. Hinde, M. Dasgupta, E. C. Simpson, D. Y. Jeung, C. Simenel, B. M. A. Swinton-Bland, E. Williams, I. P. Carter, K. J. Cook, H. M. David, C. E. Düllmann, J. Khuyagbaatar, B. Kindler, B. Lommel, E. Prasad, C. Sengupta, J. F. Smith, K. Vo-Phuoc, J. Walshe, and A. Yakushev, Phys. Rev. Lett. **122**, 232503 (2019).
[8] A. B. Balantekin and N. Takigawa, Rev. Mod. Phys. **70**, 77 (1998).
[9] K. Hagino and N. Takigawa, Phys. Rev. C **58**, 2872 (1998).
[10] K. Hagino, N. Rowley, and A. Kruppa, Comput. Phys. Commun. **123**, 143 (1999).
[11] M. Dasgupta, D. J. Hinde, N. Rowley, and A. M. Stefanini, Annu. Rev. Nucl. Part. Sci. **48**, 401 (1998).
[12] K. Hagino, S. Yusa, and N. Rowley, Nucl. Phys. A **834**, 135c (2010).
[13] M. Tokieda and K. Hagino, Phys. Rev. C **95**, 054604 (2017).
[14] G. Adamian, N. Antonenko, and W. Scheid, Nucl. Phys. A **618**, 176 (1997).
[15] P. Fröbrich, Phys. Rep. **116**, 337 (1984).
[16] G. Giardina, F. Hanappe, A. Muminov, A. Nasirov, and L. Stuttgè, Nucl. Phys. A **671**, 165 (2000).
[17] V. E. Oberacker, A. S. Umar, and C. Simenel, Phys. Rev. C **90**, 054605 (2014).
[18] A. S. Umar, V. E. Oberacker, and C. Simenel, Phys. Rev. C **92**, 024621 (2015).
[19] K. Sekizawa and K. Hagino, Phys. Rev. C **99**, 051602(R) (2019).
[20] J. Birkelund, L. Tubbs, J. Huizenga, J. De, and D. Sperber, Phys. Rep. **56**, 107 (1979).
[21] A. Nasirov, A. Fukushima, Y. Toyoshima, Y. Aritomo, A. Muminov, S. Kalandarov, and R. Utamuratov, Nucl. Phys. A **759**, 342 (2005).
[22] R. Beck and D. Gross, Phys. Lett. B **47**, 143 (1973).
[23] D. Gross and L. Satpathy, Phys. Lett. B **110**, 31 (1982).
[24] W. J. Świątecki, K. Siwek-Wilczyńska, and J. Wilczyński, Phys. Rev. C **71**, 014602 (2005).
[25] K. Hagino, Phys. Rev. C **98**, 014607 (2018).
[26] P. Fröbrich and I. Gontchar, Phys. Rep. **292**, 131 (1998).
[27] P. Fröbrich, Phys. Lett. B **122**, 338 (1983).
[28] C. Y. Wong, Phys. Rev. Lett. **31**, 766 (1973).
[29] N. D. Mavlitov, P. Fröbrich, and I. I. Gonchar, Z. Phys. A **342**, 195 (1992).
[30] J. Tōke, R. Bock, G. Dai, A. Gobbi, S. Gralla, K. Hildenbrand, J. Kuzminski, W. Müller, A. Olmi, H. Stelzer, B. Back, and S. Bjørnholm, Nucl. Phys. A **440**, 327 (1985).
[31] C. R. Morton, A. C. Berriman, M. Dasgupta, D. J. Hinde, J. O. Newton, K. Hagino, and I. J. Thompson, Phys. Rev. C **60**, 044608 (1999).
[32] A. J. Pacheco, J. O. Fernández Niello, D. E. DiGregorio, M. di Tada, J. E. Testoni, Y. Chan, E. Chávez, S. Gazes, E. Plagnol, and R. G. Stokstad, Phys. Rev. C **45**, 2861 (1992).
[33] R. Bock, Y. Chu, M. Dakowski, A. Gobbi, E. Grosse, A. Olmi, H. Sann, D. Schwalm, U. Lynen, W. Müller, S. Bjørnholm, H. Esbensen, W. Wölfli, and E. Morenzoni, Nucl. Phys. A **388**, 334 (1982).
[34] H.-G. Clerc, J. Keller, C.-C. Sahm, K.-H. Schmidt, H. Schulte, and D. Vermeulen, Nucl. Phys. A **419**, 571 (1984).
[35] V. Weisskopf, Phys. Rev. C **52**, 295 (1937).